








A fungal tolerance trait and selective inhibitors proffer HMG-CoA reductase as a herbicide mode-of-action

Received: 30 May 2022

Accepted: 7 September 2022

Published online: 22 September 2022

 Check for updatesJoel Haywood ^{1,2} ✉, Karen J. Breese ², Jingjing Zhang ², Mark T. Waters ², Charles S. Bond ², Keith A. Stubbs ² & Joshua S. Mylne ^{1,2} ✉

Decades of intense herbicide use has led to resistance in weeds. Without innovative weed management practices and new herbicidal modes of action, the unabated rise of herbicide resistance will undoubtedly place further stress upon food security. HMGR (3-hydroxy-3-methylglutaryl-coenzyme A reductase) is the rate limiting enzyme of the eukaryotic mevalonate pathway successfully targeted by statins to treat hypercholesterolemia in humans. As HMGR inhibitors have been shown to be herbicidal, HMGR could represent a mode of action target for the development of herbicides. Here, we present the crystal structure of a HMGR from *Arabidopsis thaliana* (AtHMGR1) which exhibits a wider active site than previously determined structures from different species. This plant conserved feature enables the rational design of specific HMGR inhibitors and we develop a tolerance trait through sequence analysis of fungal gene clusters. These results suggest HMGR to be a viable herbicide target modifiable to provide a tolerance trait.

As herbicide resistance continues to rise, the efficacy of herbicides has diminished¹ such that new modes of action are desperately needed. Only one new herbicide mode of action has been brought to market in almost 40 years². Weeds are yet to evolve significant resistance to clomazone and bixlozone¹, two herbicides that disrupt isoprenoid biosynthesis by targeting the enzyme 1-deoxy-D-xylulose-5-phosphate synthase³. Found in all kingdoms of life, isoprenoid biosynthesis is crucial for the synthesis of lipids, hormones, vitamins and defence compounds^{4–6}. The biosynthetic route differs between kingdoms; most animals, fungi, protists and archaea use a mevalonate (MVA) pathway, whereas most Gram-negative bacteria including cyanobacteria use a methylerythritol phosphate (MEP) pathway⁷. Through a shared evolutionary history with cyanobacteria, plants use both pathways^{7–11} compartmentalised to the cytosol (MVA) or plastids (MEP)^{12–14}. None of the known modes of action for any of the commercial herbicides affect the MVA pathway¹. An important enzyme in the MVA pathway is HMGR, which is a highly regulated^{15–19}, the rate-limiting enzyme of the MVA pathway and is the target of the group of

hypercholesterolaemia therapeutics known as statins^{20,21}. Two classes (I and II) of HMGR have been defined²² based on the differences between the catalytic core domain structure^{23,24}, the presence of an N-terminal membrane domain of between two (plants) and eight (human) membrane-spanning helices in the majority of class I enzymes^{20,25}, and the varied NAD(P)H cofactor preference²⁶. HMGR regulation appears to be conserved between humans and plants with the N-terminus regulated by ubiquitination whereas catalytic core activity is regulated by phosphorylation⁷. Many of the regulatory proteins differ, however, and this is further complicated by plants having multiple copies or isoforms plus a wide variety of external signals modifying expression, such as light and herbivory^{7,27}.

The first potent statin inhibitor of HMGR discovered was mevastatin, isolated from *Penicillium citrinum* in 1976²⁸. Lovastatin, isolated from *Aspergillus terreus* in 1978, became the first commercial statin in 1987²⁹. Second-generation statins have been semi-synthetic or synthetic products²⁹, but all statins competitively inhibit HMGR via a HMG-like moiety and a variable hydrophobic group that together give

¹Centre for Crop and Disease Management, School of Molecular and Life Sciences, Curtin University, Bentley, Perth, WA 6102, Australia. ²School of Molecular Sciences, The University of Western Australia, 35 Stirling Highway, Crawley, Perth, WA 6009, Australia. ✉ e-mail: joel.haywood@curtin.edu.au; josh.mylne@curtin.edu.au

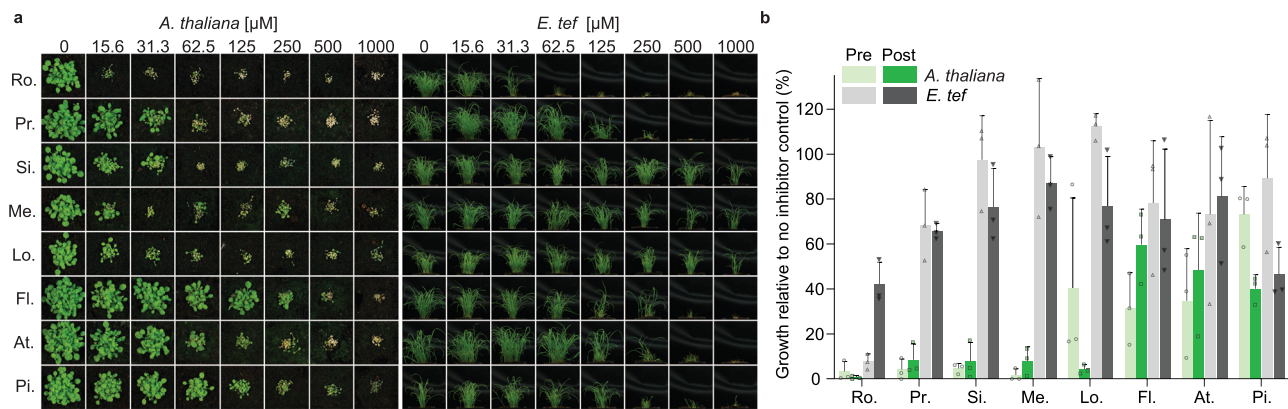


Fig. 1 | Herbicidal activity of statins varies between a model dicot and a monocot. a Representative images from the post-emergence treatment of a model dicot, *A. thaliana*, and pre-emergence treatment of the monocot *E. tef*, with statins: rosuvastatin (Ro.), pravastatin (Pr.), simvastatin (Si.), mevastatin (Me.), lovastatin (Lo.), fluvastatin (Fl.), atorvastatin (At.) and pitavastatin (Pi.). **b** *A. thaliana* (green)

and *E. tef* (grey) treated with a range of statins at 62.5 μM pre- (light colour) and post-emergence (dark colour) on soil. Inhibition was quantified using a green pixel area and plotted as a percentage of no-inhibitor control. $n = 3$ replicates with the mean \pm standard deviation (s.d.). Source data are provided as a Source Data file.

affinities to HMGR that are 10,000-fold higher than HMG-CoA³⁰. Lovastatin and mevastatin, as well as the semi-synthetic pravastatin and synthetic atorvastatin are all known to be herbicidal^{31–33}. HMGR might have been overlooked as a herbicide target due to potential off-target risks arising from its conservation in humans and the antimicrobial activity of statins³⁴, but recently developed selective insecticides against HMGR illustrate the potential to develop HMGR herbicides³⁵.

Here, we solve crystal structures for a plant HMGR in *apo* form and complexed with a statin. These structures reveal a wider active site conserved in plants compared to other organisms. By rational design we develop statin derivatives with over 20-fold specificity for the plant over the human enzyme and, which importantly, retain herbicidal activity. By comparing the AtHMGI structure to fungal HMGR genes in biosynthetic clusters for natural statins, we demonstrate a single amino acid change confers statin tolerance *in vitro* and *in planta*. Together these findings suggest HMGR is a viable target for herbicide development.

Results

Statins range in herbicidal activity

Previous studies have shown several statins to exhibit herbicidal activity against several plant species including *Lemna gibba*, *Raphanus sativus*, *Scoparia dulcis* and *A. thaliana*^{31–33,36,37}. However, there is a lack of comparative data regarding the herbicidal efficacy of statins especially for second-generation, synthetic statins. To assess herbicidal activity, we treated a model dicot and a monocot (*A. thaliana* and *Eragrostis tef*, respectively) with a dose range of eight commercially available statins on soil, pre- and post-emergence (Fig. 1). All statins were more herbicidal against the dicot and in general were more effective post-emergence. In line with their physicochemical properties more closely matching those of post-emergence herbicides (Supplementary Fig. 1a). The synthetic statin rosuvastatin was the most herbicidal statin being lethal to *A. thaliana* at $\sim 15 \mu\text{M}$ without formulation beyond including a wetting agent. Given that under the same conditions formulated glyphosate (Roundup®) is lethal at $\sim 35 \mu\text{M}$ (Supplementary Fig. 1b, c), we surmised that HMGR could represent a potential herbicide target.

Crystal structure of AtHMGI reveals scope for species selective compounds

A. thaliana has two HMGR genes with different expression patterns, but *AtHMGI* (At1g76490) is the most highly expressed³⁸. The N-terminal transmembrane domains of HMGR are highly divergent between

species and absent from class II HMGRs (Supplementary Fig. 2). By contrast, the conserved extracellular domain of AtHMGI shares $\sim 54\%$ sequence identity with HsHMGR and strictly conserved catalytic residues (Supplementary Fig. 2). To develop plant-specific statins and mitigate off-target effects, we solved the crystal structure of the core domain of *apo* AtHMGI and in complex with pitavastatin to resolutions of 1.9 and 2.1 \AA , respectively, in space group $I4_122$. Attempts were made to crystallise type I statins as described previously²⁴; however, electron density for these ligands was ambiguous. The structure of the *apo* AtHMGI displayed a single monomer in the asymmetric unit which through crystallographic symmetry forms a homotetrameric assembly (Fig. 2a), consisting of two canonical class I homodimeric HMGR folds, with high structural similarity to HsHMGR (PDB 1HWK, r.m.s.d. 1.1 \AA over 371 C α atoms, Fig. 2b).

Closer inspection of the statin-binding pocket revealed two substitutions in AtHMGI with respect to HsHMGR located at the hydrophobic CoA binding region of the active site pocket³⁹, specifically, Ile⁵⁶²/Leu⁸⁵⁷ and Ile³⁸⁹/Val⁶⁸³ in AtHMGI/HsHMGR respectively (Fig. 2c, d). Furthermore, a plant conserved Val to Pro (Pro²³⁶/Val⁵³⁰ *A. thaliana*/human) substitution at the start of the L β 1-strand is the likely cause of conformational flexibility and lack of electron density in the N α 4-L β 1 loop adjacent to the active site-delineating L β 2-L α 1 loop (Fig. 2e, Supplementary Fig. 3a, b and Supplementary Table 1). This flexibility results in the loss of a type II β -turn found within the HsHMGR L β 2-L α 1 loop that is stabilised by hydrogen bonding between a conserved Glu (Glu²³⁴/Glu⁵²⁸ AtHMGI/HsHMGR) and a Cys backbone amine (Cys²⁶⁷/Cys⁵⁶¹ AtHMGI/HsHMGR) (Fig. 2f). This altered conformation of the L β 2-L α 1 loop is not seen in any of the previous class I and II HMGR crystal structures^{24,26,30,40–50} and allows alternative conformations of the Cys²⁶⁷ residue (Fig. 2e, g, h). Importantly, the arrangement of the AtHMGI L β 2-L α 1 loop results in Glu²⁶⁵ being unable to form a hydrogen bond with the O5-hydroxyl group of the HMG moiety of statins or the equivalent thioester oxygen of HMG-CoA, as it is shifted 2.5 \AA away, creating a wider pocket (Fig. 2g). In this orientation it is more likely that Lys³⁹⁷ acts as a proton donor in the catalytic reduction of HMG-CoA to mevalonate as is suggested to occur in bacteria⁵⁰ and with molecular dynamics and quantum mechanics/molecular mechanics simulations with HsHMGR⁵¹. Together, these differences increase the solvent-accessible area of the statin pocket from $\sim 314 \text{\AA}^3$ in HsHMGR to $\sim 357 \text{\AA}^3$ in AtHMGI⁵².

The complex of AtHMGI with pitavastatin (Fig. 3a, b) revealed a binding mode highly similar to fluvastatin in HsHMGR²⁴ (Fig. 3c). Conserved polar interactions occur with the residues local to the cis

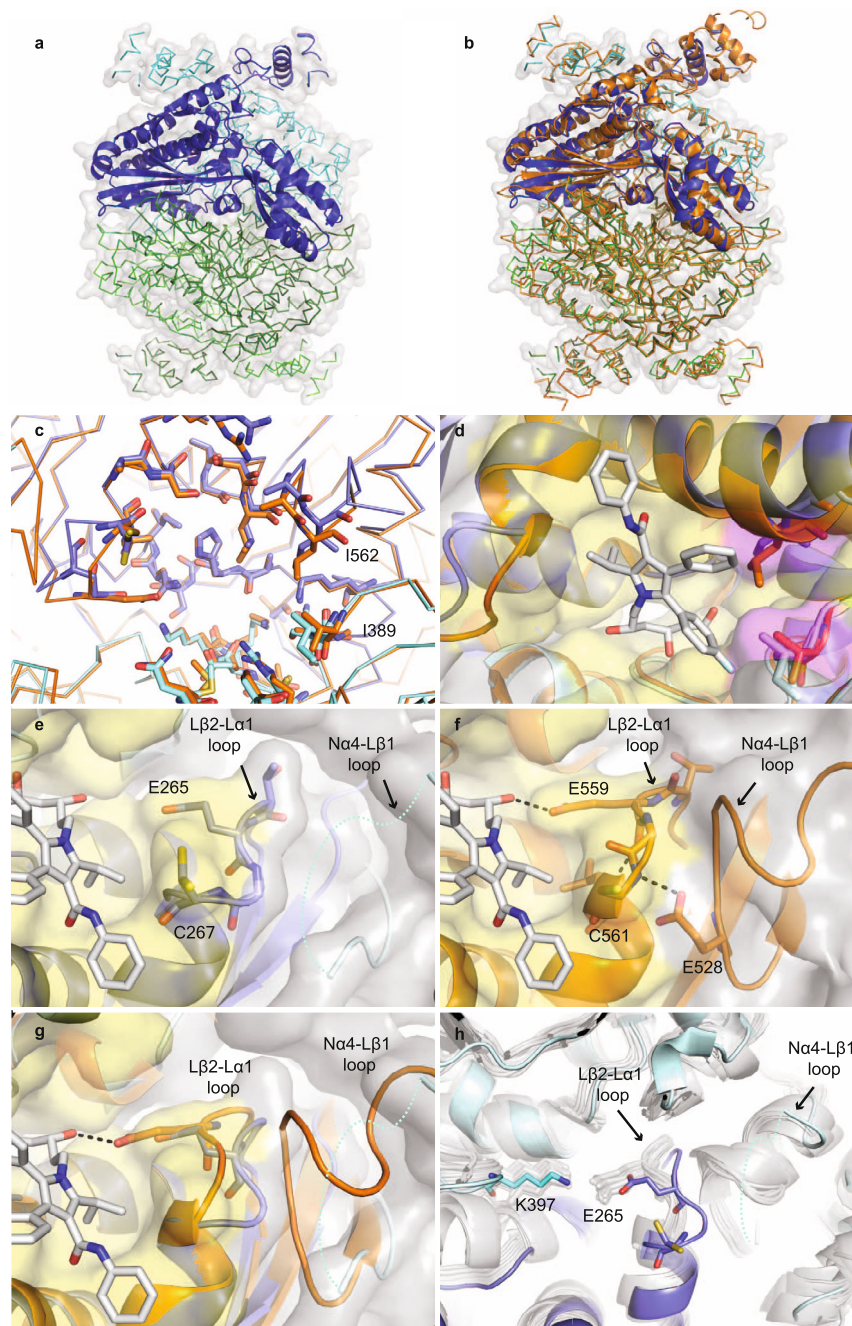


Fig. 2 | AtHMGI active site adopts a unique conformation. **a** Apo AtHMGI displays a single monomer in the asymmetric unit (dark-blue cartoon) which through crystallographic symmetry forms a homotetrameric assembly (ribbon) consisting of two canonical class I homodimeric HMGR folds (blue and green). **b** Overlay of human HMGR (orange cartoon, PDB 1HWK) with apo AtHMGI (**a**) illustrates their conserved fold. **c** AtHMGI (blue ribbon and sticks) has a highly conserved active site with HsHMGR (orange ribbon and sticks). Active site-delineating residues are shown as sticks. All residues are conserved except the two AtHMGI residues labelled. **d** Superposition of atorvastatin in the active site of AtHMGI illustrates the position of these substitutions relative to a bound statin. Conserved active site residues are shown with yellow surface and substitutions highlighted with magenta

surface. **e** Conformational flexibility in the Na4-Lβ1 loop of AtHMGI (cyan dotted line) evidenced by poor electron density is likely the result of a Pro to Val substitution. This results in the loss of a type II hydrogen bonded β-turn exhibited in HsHMGR (**f**) that allows HsHMGR E559 to hydrogen bond (dashed grey lines) to the open lactone ring of statins. Atorvastatin superimposed on apo AtHMGI (**e, g**) illustrates the equivalent residue, E265, likely too far away to H-bond to statins. Conserved active site residues (**e–g**) are shown with yellow surface. **h** Overlay of apo AtHMGI (blue cartoon and sticks) with all published structures of HMGR (grey cartoon and sticks)^{24,26,30,40–50}. To the best of our knowledge, this conformation has not been seen in any published HMGR crystal structure to date. Topology designation from HsHMGR⁴⁹.

loop Arg²⁹⁶, Ser³⁹⁰, Asp³⁹⁶, Lys³⁹⁷, Lys³⁹⁸, Asn⁴⁶¹ (HsHMGR Arg⁵⁹⁰, Ser⁶⁸⁴, Asp⁶⁹⁰, Lys⁶⁹¹, Lys⁶⁹², Asn⁷⁵⁵) and a salt-bridge between the terminal carboxylate of the HMG moiety with Lys⁴⁴¹ (HsHMGR Lys⁷³⁵) (Fig. 3a). The fluorophenyl group of pitavastatin maintains conserved stacking interactions with Arg²⁹⁶ (HsHMGR Arg⁵⁹⁰) and hydrophobic interactions between the quinoline and cyclopropyl moiety with residues

Leu²⁶⁸, Ile³⁸⁹, Leu⁵⁵⁸, Asp⁵⁶¹ (HsHMGR Leu⁵⁶², Val¹⁶⁸³, Leu⁸⁵³, Asp⁸⁵⁶). This complex structure however also revealed two notable differences between the binding mode of class II statins in AtHMGI and HsHMGR: (i) loss of hydrogen bonding to the O5-hydroxyl group of the HMG moiety of statins from Glu²⁶⁵ (HsHMGR Glu⁵⁵⁹), despite a slight shift of Glu²⁶⁵ towards the bound inhibitor (Fig. 3a and Supplementary Fig. 3c),

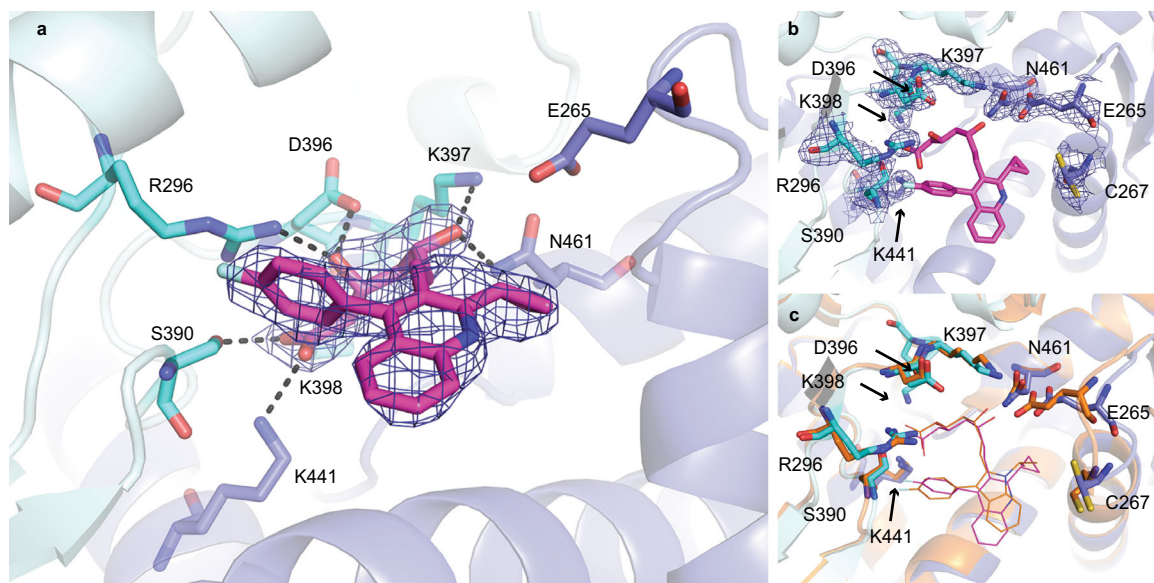


Fig. 3 | AtHMGI E265 does not hydrogen bond with statins. **a** AtHMGI with pitavastatin (magenta) bound. Residues that hydrogen bond (dashed black lines) to the HMG moiety of statins in AtHMGI are shown (blue/cyan sticks). **b** AtHMGI (blue cartoon) with pitavastatin (magenta line) bound, active site-delineating residues labelled and shown as sticks with electron density. **c** AtHMGI with pitavastatin

bound superimposed on HsHMGR bound to fluvastatin (orange cartoon and line PDB 1HWI), illustrating that binding of statins to AtHMGI is analogous to HsHMGR. Simulated annealing omit electron density maps ($2F_{\text{obs}} - F_{\text{calc}}$) contoured at 1σ level.

and (ii) the loss of hydrophobic interactions with Gly²⁶⁶, His⁴⁵⁸ and Ile⁵⁶² (HsHMGR Gly⁵⁶⁰, His⁷⁵² and Leu⁸⁵⁷). Unique hydrophobic contacts were made between pitavastatin and residues Ser²⁷¹ and Ser³⁶⁷ of AtHMGI (HsHMGR Ser⁵⁶⁵ and Ser⁶⁶¹).

Development of plant-specific analogues of statins

Our insights from the crystal structure of a model plant HMGR and the binding mode of pitavastatin provided the opportunity to rationally design plant-specific inhibitors. To this end, we sought to exploit the L β 2-L α 1 loop region of AtHMGI by developing analogues (**1–9**) of the more chemically tractable atorvastatin with modifications at the isopropyl group on the central pyrrole ring (Supplementary Fig. 3d). Activity of the atorvastatin scaffold against HsHMGR was previously found to be reduced with increasing size of the alkyl substituent⁵³ whereas the wider pocket of AtHMGI might accommodate larger groups. In addition, the loss of interactions with O5-hydroxyl group of the HMG moiety with Glu²⁶⁵ could be targeted by incorporating a hydrogen bond donor (Fig. 2e, g). Thus **1–9** were synthesised (Supplementary Method 1) and assessed for herbicidal activity on soil with *A. thaliana* (Fig. 4a) and for species-specificity against HsHMGR and AtHMGI in vitro by a fluorometric, NADPH-depletion assay (Fig. 4b–d).

Overall, atorvastatin analogues with side chains of similar length had similar herbicidal and in vitro inhibitory activity to the parent, whereas side chains longer than the isopropyl group had reduced activity (Fig. 4). Compounds **4** and **7** retained herbicidal activity and displayed a preference for AtHMGI over HsHMGR in an initial screen (Fig. 4a, b). Dose-response curves confirmed compound **7** had switched preference from human to plant when compared to atorvastatin, showing >20-fold higher specificity for AtHMGI (IC_{50} 32 nM \pm 12 nM) over HsHMGR (IC_{50} 890 nM \pm 143 nM) in vitro (Fig. 4c, d). These molecules provide a framework for the future development of plant-specific HMGR inhibitors that might exhibit stronger herbicidal activity.

Exploiting biosynthetic gene clusters to engineer statin tolerance

The most commercially successful herbicides are often paired with a tolerance trait in crops. Statins produced from fungal biosynthetic

gene clusters usually contain a copy of *HMGR* that imparts self-resistance^{54–56}, so we sought to determine the structural basis for this resistance. Sequence alignment of a *HMGR* gene (*lurA*) from the *A. terreus* genome revealed several mutations in the cluster-associated copy that were not present in the housekeeping copy (Supplementary Fig. 4). The corresponding residues of the AtHMGI crystal structure revealed a Leu (Leu⁵⁵⁸) to Thr mutation, whose equivalent was conserved in all *A. terreus* genomes in the NCBI database. The Leu to Thr mutation would likely disrupt the hydrophobic pocket essential for accommodating the decalin ring of natural statins (Fig. 5a), and so was incorporated into recombinant AtHMGI. The AtHMGI-L558T mutant was resistant to a range of statins (Fig. 5b) with >20-fold resistance to rosuvastatin in vitro (WT IC_{50} 53 nM \pm 20 nM, L558T IC_{50} >1000 nM) (Fig. 5c). Without inhibitors, AtHMGI-L558T had reduced catalytic activity (WT K_m 69 μ M \pm 19 μ M and k_{cat} 10.7 \pm 1.0 s⁻¹, L558T K_m 24 μ M \pm 16 μ M and k_{cat} 2.4 \pm 0.3 s⁻¹) (Supplementary Fig. 5), but remained within the range of previously published rates for other class I and II HMGR enzymes⁵⁷.

To validate the potential of the L558T mutation for providing a plant tolerance trait, we overexpressed full-length AtHMGI (*35S::AtHMGI*) and its equivalent with the L558T mutation (*35S::AtHMGI-L558T*) in *A. thaliana*, using a cauliflower mosaic virus (CaMV) 35S promoter. It has previously been shown that overexpressing *AtHMGI* in *A. thaliana* can give rise to a 40-fold rise in mRNA levels and a modest rise in resistance to lovastatin compared to non-transformed WT controls⁵⁸. Here we found with data collated from 19 independent T₂ *35S::AtHMGI* lines and 14 independent *35S::AtHMGI-L558T* T₂ lines that both constructs conferred similar resistance to the selectable marker hygromycin (Fig. 6a, d). However, the *35S::AtHMGI-L558T* lines were over sixfold more resistant to rosuvastatin (IC_{50} 300 μ M vs \pm 18 μ M) than *35S::AtHMGI* lines (IC_{50} 46 μ M \pm 5 μ M) and more than 100-fold more resistant than non-transformed WT (IC_{50} 3 μ M vs \pm 1 μ M) (Fig. 6b, d). Furthermore, analysis of the effects of rosuvastatin revealed *35S::AtHMGI-L558T* lines were up to 16-fold less sensitive to treatment than *35S::AtHMGI* lines (Fig. 6c). These results illustrate the potential for HMGR to have a tolerance trait and further validates the in vitro results (Fig. 5b, c).

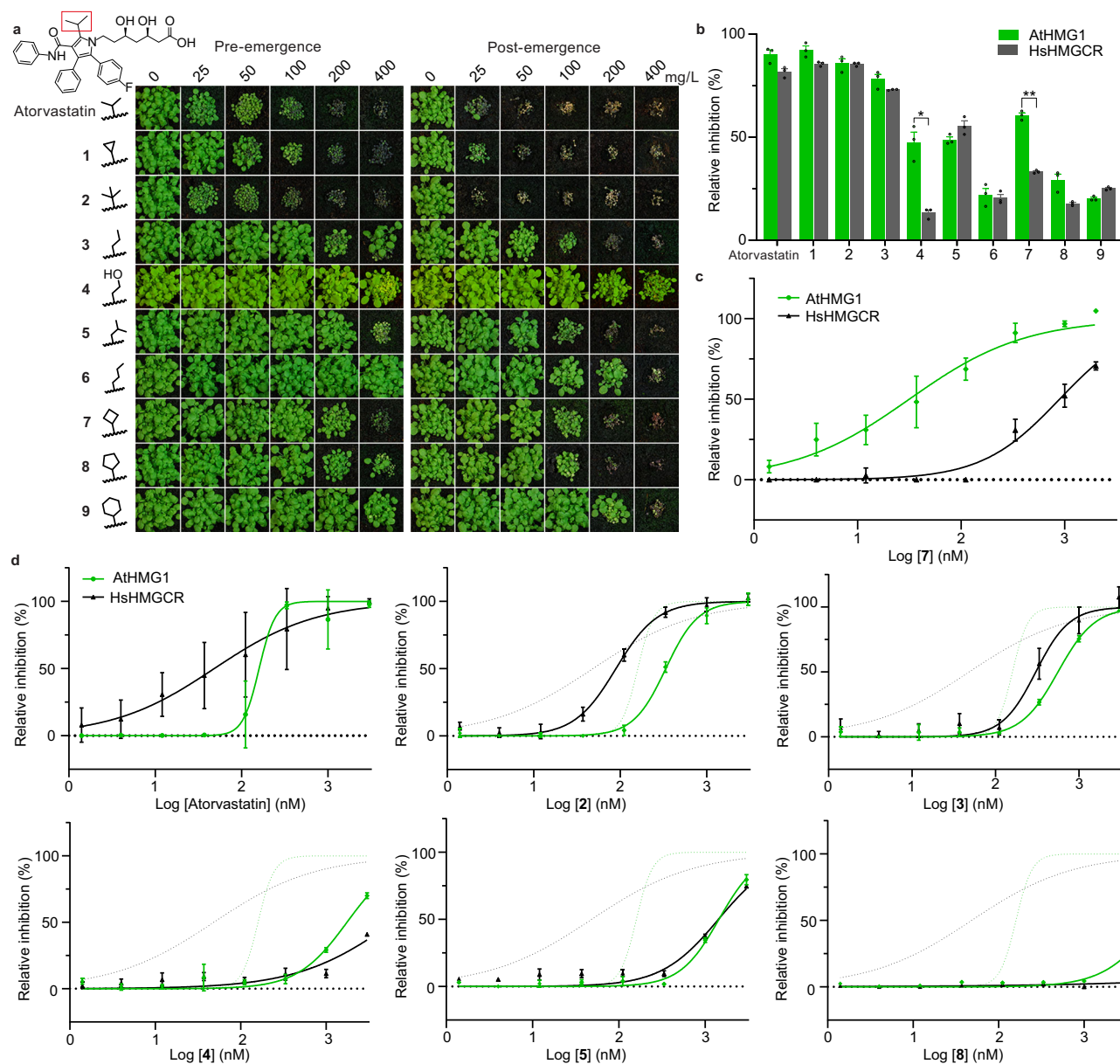


Fig. 4 | Modifying the isopropyl group of atorvastatin affects species selectivity. **a** Herbicidal activity of atorvastatin and its analogues (1–9) against *A. thaliana* with pre- and post-emergence treatments. The isopropyl moiety of atorvastatin is boxed in red. Modifications to the isopropyl region are shown. **b** Compounds 4 and 7 were selective in vitro for AtHMG1 (green bar) over HsHMGR (grey bar) at 500 nM. $n = 3$ independent reactions with the mean \pm s.d. Significance from two-tailed paired t test, values: compound 4 $t = 5.536$ $df = 2$ $P = 0.03$ (*) 95% CI [–60.92 to –7.635], compound 7 $t = 16.93$ $df = 2$ $P = 0.003$ (**) 95% CI [–34.37 to –20.44]. **c** In

vitro inhibition of AtHMG1 (green plot) and HsHMGR (grey plot) by 7 illustrating >20-fold selectivity for AtHMG1. $n = 3$ independent reactions with the mean \pm s.d. **d** Atorvastatin and analogues 2–5 and 8 were not selective for AtHMG1 in vitro. Inhibition of AtHMG1 and HsHMGR with atorvastatin inhibition profile shown as green and grey dotted lines, respectively. $n = 3$ independent reactions with the mean \pm s.d. except for a single point (AtHMG1 333 μ M atorvastatin $n = 2$). Source data are provided as a Source Data file.

Discussion

The relentless rise in herbicide-resistant weeds already poses a significant threat to global food security and as such, new herbicides with new modes of action are desperately needed. Moreover, as consumer attitudes shift, natural product ‘bioherbicides’ will rise in their appeal and currently in the USA enjoy an accelerated regulatory journey⁵⁹.

Herein, we have validated HMGR as a potential herbicide target. Using the HMGR crystal structure from a model plant we have demonstrated that, despite its overall sequence and structure conservation with HsHMGR, differences in the architecture (especially the active site) can be exploited to develop plant-specific synthetic HMGR inhibitors. The progress herein provides a basis for the discovery of natural product statins that might be suitable bioherbicides.

The differences in the architecture of AtHMG1 that allowed for species selectivity largely arise from an unusual orientation of the L β 2-L α 1 loop that is likely the result of increased flexibility in the neighbouring N α 4-L β 1 loop. The atypical orientation of the L β 2-L α 1 loop in AtHMG1 disrupts the hydrogen bonding network formed between the catalytic residues Glu²⁶⁵/Lys³⁹⁷/Asn⁴⁶¹/Asp⁴⁷³ (HsHMGR Glu⁵⁵⁹/Lys⁶⁹¹/Asn⁷⁵⁵/Asp⁷⁶⁷), thereby retaining only those hydrogen bonds that stabilise the catalytic Lys via the adjacent Asn and Asp residues. The conserved location of the catalytic Lys between AtHMG1 and other class I and II HMGRs strongly suggests this residue is responsible for polarising the carbonyl oxygen of HMG-CoA substrate and mevaldehyde intermediate, and for performing the final protonation step. Glu²⁶⁵ is not in a favourable position to hydrogen bond to either the

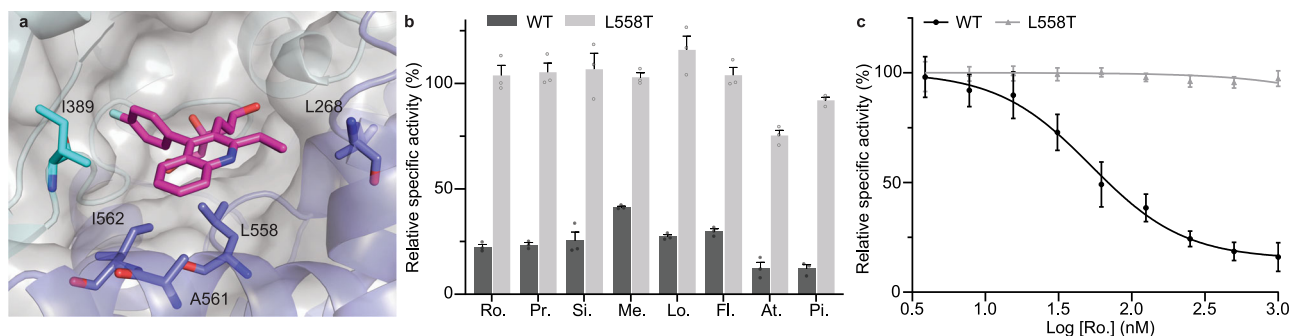


Fig. 5 | A mutation found in a statin biosynthetic cluster confers statin resistance in vitro. **a** The hydrophobic pocket in AtHMG1 delineated by labelled residues (blue sticks) with pitavastatin (magenta sticks) bound, illustrating L558 proximity to the hydrophobic ring of statins. **b** AtHMG1 with the L558T mutation (grey bar) in comparison to wild-type (black bar) retained activity in vitro in the presence of statins: rosuvastatin (Ro.), pravastatin (Pr.), simvastatin (Si.), mevastatin (Me.), lovastatin (Lo.), fluvastatin (Fl.), atorvastatin (At.) and pitavastatin (Pi.), at 500 nM. $n = 3$ independent reactions with the mean \pm s.d. **c** In vitro inhibition of WT (black plot) and L558T AtHMG1 (grey plot) by rosuvastatin revealed the L558T mutation conferred >20-fold resistance. $n = 3$ independent reactions with the mean \pm s.d. Source data are provided as a Source Data file.

mevastatin (Me.), lovastatin (Lo.), fluvastatin (Fl.), atorvastatin (At.) and pitavastatin (Pi.), at 500 nM. $n = 3$ independent reactions with the mean \pm s.d. **c** In vitro inhibition of WT (black plot) and L558T AtHMG1 (grey plot) by rosuvastatin revealed the L558T mutation conferred >20-fold resistance. $n = 3$ independent reactions with the mean \pm s.d. Source data are provided as a Source Data file.

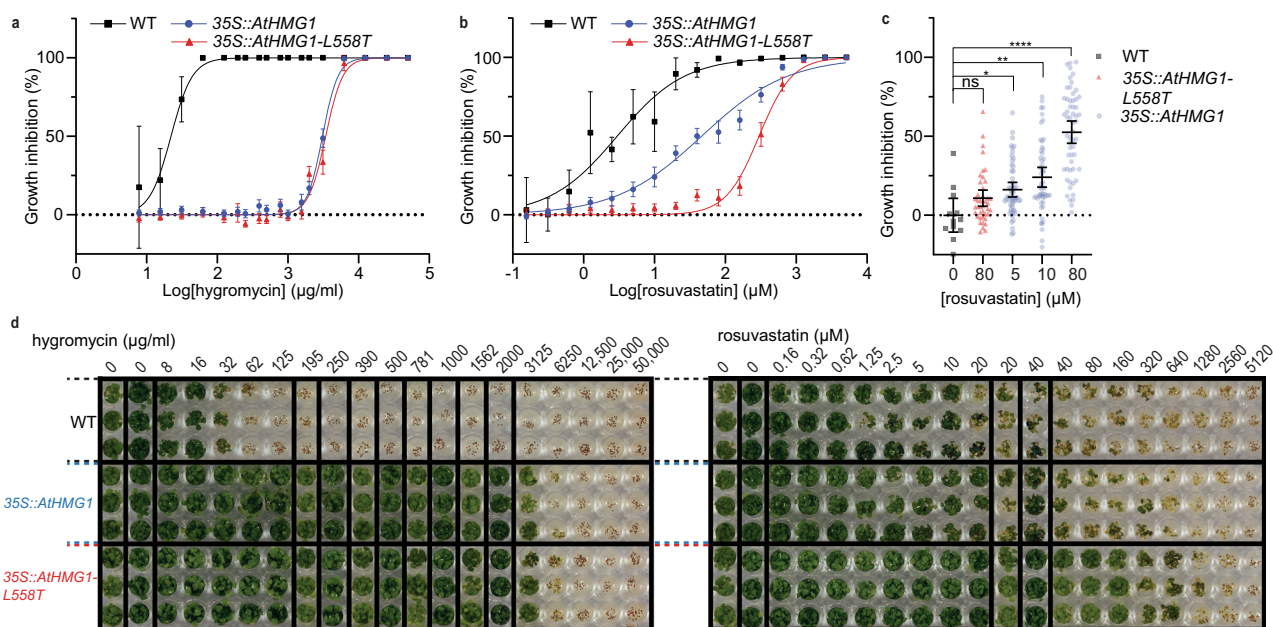


Fig. 6 | The L558T mutation gives resistance to rosuvastatin in planta. Resistance to hygromycin (**a**) and rosuvastatin (**b**, **c**) in 19 transgenic lines of *35S::AtHMG1* (blue) versus 14 *35S::AtHMG1-L558T* lines (red) and wild type (WT, black). Green pixels quantified and plotted as a percentage of no-inhibitor control. **a**, Both transgenic lines exhibited similar resistance to the hygromycin selectable marker, whereas WT was sensitive, mean \pm 95% CI. **b** *35S::AtHMG1-L558T* transgenic lines were sixfold more resistant to rosuvastatin than *35S::AtHMG1*, mean \pm 95% CI, but \pm s.d. for WT. **c** Susceptibility of transgenics to rosuvastatin illustrated *35S::AtHMG1-L558T* (red 80 μ M $n = 42$) was up to 16-fold less susceptible to rosuvastatin inhibition than *35S::AtHMG1* (blue 5 μ M $n = 54$, 10 μ M $n = 54$, 80 μ M $n = 57$) when compared to

untreated WT (black $n = 12$). Significance from one-way ANOVA with Dunnett's multiple comparison correction against a common control performed, bars represent mean \pm 95% CI. Values: 0 μ M vs 80 μ M *35S::AtHMG1-L558T* $q = 1.566$ $df = 214$ $P = 0.24$ (ns) 95% CI [-27.00 to -5.299], 0 μ M vs 5 μ M *35S::AtHMG1* $q = 2.395$ $df = 214$ $P = 0.04$ (*) 95% CI [-31.92 to -0.4293], 0 μ M vs 10 μ M *35S::AtHMG1* $q = 3.564$ $df = 214$ $P = 0.0013$ (**) 95% CI [-39.82 to -8.324], 0 μ M vs 80 μ M *35S::AtHMG1* $q = 7.829$ $df = 214$ $P = <0.0001$ (****) 95% CI [-68.29 to -36.95]. **d** Representative image of resistance to hygromycin and rosuvastatin from a single line of *35S::AtHMG1* and *35S::AtHMG1-L558T* versus WT. Source data are provided as a Source Data file.

substrate thioester oxygen or the adjacent Asp⁴⁷³, which based on HsHMGR in silico simulations (HsHMGR Glu⁵⁵⁹ and Asp⁷⁶⁷) might be expected to hydrogen bond and stabilise the mevaldyl-CoA intermediate⁵¹. Further molecular dynamics studies with AtHMG1, its substrate and cofactors might determine if the role of Glu²⁶⁵ is to hydrogen bond to Asp⁴⁷³, or to directly protonate the substrate as previous modelling studies have suggested^{60,61}.

Here, we rationally designed a compound with >20-fold preference for plant HMGR in vitro with limited modification to the parent scaffold. Modelling of atorvastatin along with compounds **4** and **7** into the active site of HsHMGR revealed a single dominant high-affinity

binding mode with a large drop in affinity to the next most favourable binding mode. Atorvastatin exhibited the highest affinity followed by compound **7** and **4** (Supplementary Fig. 6) consistent with in vitro results (Fig. 4). Modelling with AtHMG1 revealed more varied poses of the analogues, with similar affinities between the most favourable binding modes. These binding modes are possibly facilitated by a wider active site and flexibility in the L β 2-L α 1 loop region (Supplementary Fig. 3c) and might account for the difficulty we had in obtaining co-crystal structures for AtHMG1. The lower affinity for AtHMG1 than HsHMGR for compounds **4** and **7** suggests further molecular dynamics simulations and crystallographic studies may be

necessary to help reveal the molecular basis of in vitro specificity (Fig. 4). Notably, selectivity over HsHMGR was also obtained by targeting the same L β 2-L α 1 loop region in *Manuca sexta* using gem-difluoromethylenated HMGR inhibitors³⁵. Similar derivatives may also prove to be selective for plant HMGRs. Overall, the developed compounds provide a framework for further structure-based rational herbicide design targeting the L β 2-L α 1 loop region of AtHMGI, which could be validated for selectivity in mammalian in vivo studies. Greater species selectivity might be obtainable by targeting the N-terminal domain of HMGR, which is highly divergent between humans and plants and is absent from class II HMGRs. A recent crystal structure of the regulatory elements that interact with the N-terminal domain in HsHMGR and studies of compounds that increase HMGR degradation suggest that this could be an alternative mechanism to lower cholesterol levels^{16,18}. Future studies of the regulatory elements interacting with plant HMGR N-terminal domain and complexed crystal structures might in the same way also provide an avenue to develop more species-specific inhibitors of HMGR. The regulatory elements that control plant lipid metabolism might also provide new herbicidal targets, just as the proprotein convertase subtilisin/kexin type 9 and angiotensin-like 3 are providing new avenues for the treatment of hypercholesterolaemia^{62,63}.

By analysing the AtHMGI crystal structure and sequences in fungal biosynthetic gene clusters, we identified a mutation conferring statin resistance without adversely affecting catalytic activity. Over-expressing this mutant protein in *A. thaliana* demonstrated its potential as a tolerance trait, but further investigations are needed. These could include (i) the efficacy of this protein mutant in different species; (ii) optimisation of expression and regulation, by modifying the N-terminal domain; (iii) its effects on sterol levels and seed set⁶⁴; and (iv) determining what HMGR inhibitor residues remain in the treated crop or soil. Future studies might also focus on other residues that potentially impart resistance, such as the end region of the S β 4 strand (residues 387–390), that show conservation in putative resistance genes from *Penicillium citrinum* and *Xylaria grammica* and could affect binding of the butyryl group of natural statins. We envisage that the development and discovery of new, natural product herbicides^{65,66} might also benefit from a similar approach to engineering resistance alleles from biosynthetic gene clusters containing compounds or targets of interest.

Methods

Herbicidal activity assay

Approximately 30 seeds of *A. thaliana* (accession Col-0) or *E. tef* were sown in 63 × 63 × 59 mm pots of Irish peat (Bord na Móna Horticulture Ltd, Newbridge, Ireland). Seeds were incubated in the dark for 3 days at 4 °C to synchronise germination. A single pre-emergence treatment (day 0) was performed when these seeds were transferred to a growth room at 22 °C with a 16:8 h light:dark photoperiod and 60% relative humidity. Two post-emergence treatments were performed following emergence of the seedlings (day 1) at days 4 and 7. Plants were watered accordingly throughout the experiment to maintain adequate moisture and photographed on day 16. Treatments were conducted with rosuvastatin, simvastatin, fluvastatin, atorvastatin (AK Scientific), pravastatin (BOC Sciences), lovastatin (Sapphire Bioscience), mevastatin, pitavastatin (Focus Bioscience), glyphosate, RoundUp® and atorvastatin analogues (1–9). To treat, 0.5 mL of each compound in a final concentration of 2% dimethyl sulfoxide (DMSO) and 0.02% Brushwet (SST Dandenong, Australia) was pipetted onto seedlings. Full experimental details and characterisation of atorvastatin analogue 1–9 synthesis can be found in Supplementary Method 1 and Supplementary Figs. 7–62. Growth inhibition was quantified by detecting green pixels for healthy seedlings using ImageJ (National Institutes of Health, 1.53 v) and the 'Threshold Colour' plug-in with the following settings: hue 50–110, saturation 125–255, brightness 30–255⁶⁷. Images were

converted into 8-bit format, and pixels measured over the same area. Data were normalised to a negative control to provide percentage inhibition.

HMG-CoA reductase expression and purification

An *E. coli* codon-optimised DNA sequence encoding the conserved extracellular region of AtHMGI (Uniprot P14891, AtIg76490, residues 121–592) was cloned into pQE30 (Qiagen) following an N-terminal His₆-tag and tobacco etch virus cleavage site. The protein was expressed in the T7 SHuffle Express strain of *E. coli* (New England Biolabs) transformed with pREP4 (Qiagen) with the proteins expressed and purified as previously described⁶⁸. Briefly, cultures were grown in lysogeny broth containing 100 μ g/mL ampicillin and 35 μ g/mL kanamycin at 30 °C to an OD₆₀₀ of 0.8–1.0. Cells were cooled to 16 °C before the expression was induced with 0.1 mM isopropyl β -D-1-thiogalactopyranoside. Following overnight culture, cells were harvested by centrifugation and lysed by ultrasonication in 100 mM HEPES (pH 7.5), 150 mM sodium chloride, 5 mM dithiothreitol, 0.1% Triton X-100. Lysed cells were then centrifuged (15,000 \times g) and the supernatant was incubated in 30 mL batches with Ni-NTA resin overnight at 4 °C. The resin was then washed with 50 mL of 100 mM HEPES (pH 7.5), 150 mM sodium chloride, 5 mM dithiothreitol followed by 50 mL of 100 mM HEPES (pH 7.5), 150 mM sodium chloride, 5 mM dithiothreitol, 20 mM imidazole. The protein was then eluted with 50 mL of 100 mM HEPES (pH 7.5), 150 mM sodium chloride, 5 mM dithiothreitol, 300 mM imidazole. Eluted protein was concentrated with a 30 kDa centrifugal filter unit (Millipore) and purified by size-exclusion chromatography (HiLoad 16/600 Superdex 200) in 100 mM HEPES (pH 7.5), 150 mM sodium chloride, 5 mM dithiothreitol. The protein was assessed for purity by SDS-PAGE, and protein concentration was determined by spectrophotometry.

In vitro HMGR assay

AtHMGI described above and human HMGR (HsHMGR, Uniprot P04035, residues 441–888, cloned as above) were purified as above, and activity was determined by spectrophotometric measurement of the decrease in absorbance at 340 nm that occurs with NADPH oxidation in the presence of substrate HMG-CoA (Sigma-Aldrich). Reactions were performed with an assay buffer consisting of 150 mM sodium chloride, 5 mM dithiothreitol, 50 mM HEPES pH 7.4 and 2% DMSO. For kinetics determinations, a final concentration of 150 nM enzyme was incubated at 37 °C in 300 μ M NADPH and different concentrations of HMG-CoA. Non-linear regression analysis was performed with GraphPad Prism 9 by plotting the initial reaction rates, v_0 , interpolated from a standard curve against the substrate concentration. The Michaelis–Menten constant, K_m , was determined by fitting the data with a Michaelis–Menten equation and values for k_{cat} were calculated by dividing V_{max} by the molar enzyme concentration. To calculate relative specific activity, 500 nM of test compounds were pre-incubated at 37 °C with enzyme and 300 μ M NADPH for 15 min before adding HMG-CoA to 200 μ M. Resultant values were background subtracted and normalised to the average of the no-inhibitor control. For IC₅₀ determinations, the same protocol was used, but varying inhibitor concentrations. Rosuvastatin data were plotted with a four-parameter (WT), and normalised response (L558T) non-linear regression model and atorvastatin and analogues were plotted with a normalised response with variable slope non-linear regression model.

Crystallisation and data collection

The C-terminal core residues of AtHMGI (residues 121–576) were cloned and purified as above. The core domain was concentrated to 10–15 mg/mL and used immediately for crystallisation. Crystal screening was performed with 96-well Intelli-Plates (Hampton Research) with 80 μ L of reservoir solution using the sitting-drop vapour diffusion method at 16 °C. Crystals were obtained with a

Table 1 | Crystallography data collection and refinement statistics

Data collection	<i>apo</i> HMG1	HMG1-pitavastatin
Space group	I 4 ₁ 2 2	I 4 ₁ 2 2
Unit cell dimensions		
a, b, c (Å)	85.58, 85.58, 266.65	85.55, 85.55, 265.15
α, β, γ (°)	90.00, 90.00, 90.00	90.00, 90.00, 90.00
Wavelength	0.9537	0.9537
Resolution (Å)	1.7	2.1
R _{merge} (%)	11 (434) [*]	25 (267)
I/σI	14.8 (1.63)	12 (1.1)
Completeness (%)	100 (99.9)	60.9 (11.6) spherical 91.6 (60.7) ellipsoidal
Redundancy	13.3 (11.6)	18.2 (14)
CC 1/2	1.00 (0.549)	0.996 (0.341)
Refinement		
Resolution (Å)	45.30-1.90	45.07-2.13
No. of reflections	39555	17133
R _{work} /R _{free}	20.7/24.3	22.0/26.1
No. of atoms	5398	5054
Protein	5307	4971
Water	91	19
Ligand		64
Wilson B (Å ²)	51.0	29.7
Average refined B-factor (Å ²)		
Protein only (Å ²)	51.0	29.3
Water (Å ²)	53.5	12.8
Ligand (Å ²)		45.0
Bond lengths (Å)	0.01	0.01
Bond angles (°)	1.36	1.55
Ramachandran analysis		
Favoured (%)	97	94
Allowed (%)	3	6
Outliers (%)	0	0
PDB accession	7ULI	8ECG

*Numbers in parentheses refer to the highest resolution bin.

mother-liquor of 0.2 M ammonium sulphate, 0.1 M HEPES and 35% w/v poly(acrylic acid sodium salt) 2100 from the Molecular Dimensions MIDASplus™ screen. Crystals were optimised using a 96-well additive screen, and well-diffracting crystals obtained in the same plates with a 1 μL droplet containing 0.6 μL of the above mother-liquor, 0.3 μL of protein and 0.1 μL of Hampton Research additive screen. Crystals used for inhibitor soaks were grown with the additives 40% v/v pentaerythritol ethoxylate (3/4 EO/OH) and 0.1 M iron(III) chloride hexahydrate. Inhibitor soaks were carried out in the same mother-liquor with 1 mg/mL of inhibitors. Single crystals were quickly soaked in mother-liquor containing 25% glycerol as a cryoprotectant before being flash frozen and stored in liquid nitrogen. Data collection was performed at 100 K on the Australian MX2 (micro-focus) beamline⁶⁹ with 1.9 Å resolution for the *apo* form and 2.1 Å for inhibitor complexed AtHMG1.

Crystal structure determination, refinement and model building
Apo and complexed AtHMG1 diffraction data were processed using XDS and scaled with AIMLESS from CCP4^{70,71}. A sequence alignment of AtHMG1 and HsHMGCR was generated using ClustalO and used to create a search model of AtHMG1 based on the last common atom of PDB 1HW8. This model was then used for molecular replacement with PHASER from CCP4⁷². Manual building and refinement were

performed in iterative cycles with Coot and REFMAC5 using the CCP4 programme suite⁷³. Structure analysis and validation were carried out with Coot and MolProbity⁷⁴. The refined AtHMG1 structure was then used as a search model for molecular replacement with data from inhibitor complexed crystals. Crystallographic data and refinement statistics are summarised in Table 1 with Ramachandran plot values calculated from CCP4. Coordinates and structure factors were deposited into the PDB under accession codes 7ULI and 8ECG. Figures illustrating the structures were generated using PyMol.

In planta statin resistance assay

DNA encoding the full-length AtHMG1 protein (Uniprot P14891, residues 1–592) and the corresponding L558T mutant were cloned into a derivative of the pMDC43 binary vector⁷⁵ to yield *35 S::AtHMG1* and *35 S::AtHMG1-L558T* transgenes, respectively. These constructs were then introduced into *Agrobacterium tumefaciens* strain LBA4404 and separately used to transform *A. thaliana* by the floral dip method^{76,77}. Seeds (T_{0/1}) of transformed plants were collected and surface sterilised using 600 μL 70% ethanol, 750 μL 100% ethanol and soaked in 800 μL 50% bleach for 8 min, before washing with 800 μL sterile water and resuspension with 0.1% agar. Selection was performed on 30 μg/mL hygromycin growth medium (1% agar, 1% glucose, 0.45% Murashige & Skoog salts with vitamins, 0.3% 2-(N-morpholino)-ethanesulfonic acid (MES) (v/v), pH 5.7) in a growth room at 22 °C with 16:8 h light:dark photoperiod and 60% relative humidity. Surviving plants were transferred to 63 × 63 × 59 mm pots of Irish peat and grown to maturity in the same growth conditions. Seeds from plants with an adequate seed yield were then sterilised and selected again as described above with 30 μg/mL hygromycin growth medium. Seeds (T₂) from 22 lines of *35 S::AtHMG1* and 15 lines of *35 S::AtHMG1-L558T* plants that exhibited approximately 3:1 segregation ratio of hygromycin resistant:sensitive were then sown (-15 seeds/well, n = 3 replicates), along with wild-type (WT) *A. thaliana*, on sterile 96-well microplates with 0.25 mL/well growth medium containing a low dose range serial dilution of 8–2000 μg/mL hygromycin and of 0.16–40 μM rosuvastatin (final concentration 2% DMSO) with respective media only controls, and then again on a second higher dose range of 195–50,000 μg/mL hygromycin and of 20–5120 μM rosuvastatin (final concentration 2% DMSO). Plates were sealed with porous tape and grown for a minimum of 10 days with the growth conditions described above. Plates were then imaged, and growth quantified using ImageJ as described above. Total green pixels were normalised against negative controls for the respective lines (2% DMSO and water) to provide percentage inhibition. Three of 22 lines of *35 S::AtHMG1* and 1 of 15 lines of *35 S::AtHMG1-L558T* plants were excluded from further analysis based on poor growth of the negative control or for displaying low hygromycin resistance. One of 19 *35 S::AtHMG1* lines and 2 of the 14 *35 S::AtHMG1-L558T* lines had data only for the higher dose range of hygromycin and rosuvastatin. For IC₅₀ determinations, all data were respectively combined from 19 lines of *35 S::AtHMG1*, 14 lines of *35 S::AtHMG1-L558T* and WT *A. thaliana*. Growth inhibition at varying concentrations of hygromycin and rosuvastatin were plotted with a four-parameter non-linear regression model using GraphPad Prism 9.

Reporting summary

Further information on research design is available in the Nature Research Reporting Summary linked to this article.

Data availability

The refined structural protein models of *apo* HMG1 and HMG1-pitavastatin are available at PDB under accession codes 7ULI and 8ECG, respectively. Source data are provided with this paper.

References

1. Heap, I. The international survey of herbicide resistant weeds. Accessed 1 May 2022. <https://www.weedscience.org> (2022).
2. Shino, M., Hamada, T., Shigematsu, Y., Hirase, K. & Banba, S. Action mechanism of bleaching herbicide cyclopyrimorate, a novel homogentisate solanesyltransferase inhibitor. *J. Pestic. Sci.* **43**, 233–239 (2018).
3. Ferhatoglu, Y. & Barrett, M. Studies of clomazone mode of action. *Pestic. Biochem. Physiol.* **85**, 7–14 (2006).
4. Lange, B. M., Rujan, T., Martin, W. & Croteau, R. Isoprenoid biosynthesis: the evolution of two ancient and distinct pathways across genomes. *Proc. Natl Acad. Sci. USA* **97**, 13172–13177 (2000).
5. Summons, R. E., Jahnke, L. L., Hope, J. M. & Logan, G. A. 2-Methylhopanoids as biomarkers for cyanobacterial oxygenic photosynthesis. *Nature* **400**, 554–557 (1999).
6. Brocks, J. J., Logan, G. A., Buick, R. & Summons, R. E. Archean molecular fossils and the early rise of eukaryotes. *Science* **285**, 1033–1036 (1999).
7. Vranová, E., Coman, D. & Grussem, W. Network analysis of the MVA and MEP pathways for isoprenoid synthesis. *Annu. Rev. Plant Biol.* **64**, 665–700 (2013).
8. Rodríguez-Concepción, M. et al. Distinct light-mediated pathways regulate the biosynthesis and exchange of isoprenoid precursors during *Arabidopsis* seedling development. *Plant Cell* **16**, 144–156 (2004).
9. Hemmerlin, A. et al. Cross-talk between the cytosolic mevalonate and the plastidial methylerythritol phosphate pathways in tobacco bright yellow-2 cells. *J. Biol. Chem.* **278**, 26666–26676 (2003).
10. Laule, O. et al. Crosstalk between cytosolic and plastidial pathways of isoprenoid biosynthesis in *Arabidopsis thaliana*. *Proc. Natl Acad. Sci. USA* **100**, 6866–6871 (2003).
11. Nagata, N., Suzuki, M., Yoshida, S. & Muranaka, T. Mevalonic acid partially restores chloroplast and etioplast development in *Arabidopsis* lacking the non-mevalonate pathway. *Planta* **216**, 345–350 (2002).
12. Hoshino, Y. & Gaucher, E. A. On the origin of isoprenoid biosynthesis. *Mol. Biol. Evolution* **35**, 2185–2197 (2018).
13. Zeng, L. & Dehesh, K. The eukaryotic MEP-pathway genes are evolutionarily conserved and originated from *Chlamydia* and cyanobacteria. *BMC Genomics* **22**, 1–12 (2021).
14. Lichtenthaler, H. K., Schwender, J., Disch, A. & Rohmer, M. Biosynthesis of isoprenoids in higher plant chloroplasts proceeds via a mevalonate-independent pathway. *FEBS Lett.* **400**, 271–274 (1997).
15. Goldstein, J. L. & Brown, M. S. Regulation of the mevalonate pathway. *Nature* **343**, 425–430 (1990).
16. Jiang, S.-Y. et al. Discovery of a potent HMG-CoA reductase degrader that eliminates statin-induced reductase accumulation and lowers cholesterol. *Nat. Commun.* **9**, 1–13 (2018).
17. Burg, J. S. & Espenshade, P. J. Regulation of HMG-CoA reductase in mammals and yeast. *Prog. Lipid Res.* **50**, 403–410 (2011).
18. Yan, R. et al. A structure of human Scap bound to Insig-2 suggests how their interaction is regulated by sterols. *Science* **371**, eabb2224 (2021).
19. Seydel, P. & Dörnenburg, H. Establishment of in vitro plants, cell and tissue cultures from *Oldenlandia affinis* for the production of cyclic peptides. *Plant Cell, Tissue Organ Cult.* **85**, 247–255 (2006).
20. Friesen, J. A. & Rodwell, V. W. The 3-hydroxy-3-methylglutaryl coenzyme-A (HMG-CoA) reductases. *Genome Biol.* **5**, 248 (2004).
21. Grundy, S. M. HMG-CoA reductase inhibitors for treatment of hypercholesterolemia. *N. Engl. J. Med.* **319**, 24–33 (1988).
22. Bochar, D. A., Stauffacher, C. V. & Rodwell, V. W. Sequence comparisons reveal two classes of 3-hydroxy-3-methylglutaryl coenzyme A reductase. *Mol. Genet. Metab.* **66**, 122–127 (1999).
23. Lawrence, C. M., Rodwell, V. W. & Stauffacher, C. V. Crystal structure of *Pseudomonas mevalonii* HMG-CoA reductase at 3.0 angstrom resolution. *Science* **268**, 1758–1762 (1995).
24. Istvan, E. S. & Deisenhofer, J. Structural mechanism for statin inhibition of HMG-CoA reductase. *Science* **292**, 1160–1164 (2001).
25. Learned, R. M. & Fink, G. R. 3-Hydroxy-3-methylglutaryl-coenzyme A reductase from *Arabidopsis thaliana* is structurally distinct from the yeast and animal enzymes. *Proc. Natl Acad. Sci. USA* **86**, 2779–2783 (1989).
26. Ragwan, E. R., Arai, E. & Kung, Y. New crystallographic snapshots of large domain movements in bacterial 3-hydroxy-3-methylglutaryl coenzyme A reductase. *Biochemistry* **57**, 5715–5725 (2018).
27. Rodríguez-Concepción, M. & Boronat, A. Breaking new ground in the regulation of the early steps of plant isoprenoid biosynthesis. *Curr. Opin. Plant Biol.* **25**, 17–22 (2015).
28. Endo, A., Kuroda, M. & Tsujita, Y. ML-236A, ML-236B, and ML-236C, new inhibitors of cholesterol synthesis produced by *Penicillium citrinum*. *J. Antibiotics* **29**, 1346–1348 (1976).
29. Tobert, J. A. Lovastatin and beyond: the history of the HMG-CoA reductase inhibitors. *Nat. Rev. Drug Discov.* **2**, 517–526 (2003).
30. Taberner, L., Rodwell, V. W. & Stauffacher, C. V. Crystal structure of a statin bound to a class II hydroxymethylglutaryl-CoA reductase. *J. Biol. Chem.* **278**, 19933–19938 (2003).
31. Bach, T. J. & Lichtenthaler, H. K. Inhibition by mevinolin of plant growth, sterol formation and pigment accumulation. *Physiologia Plant.* **59**, 50–60 (1983).
32. Kasahara, H. et al. Contribution of the mevalonate and methylerythritol phosphate pathways to the biosynthesis of gibberellins in *Arabidopsis*. *J. Biol. Chem.* **277**, 45188–45194 (2002).
33. Nkembo, M. K., Lee, J.-B., Nakagiri, T. & Hayashi, T. Involvement of 2-C-methyl-D-erythritol-4-phosphate pathway in biosynthesis of aphidicolin-like tetracyclic diterpene of *Scoparia dulcis*. *Chem. Pharm. Bull.* **54**, 758–760 (2006).
34. Jerwood, S. & Cohen, J. Unexpected antimicrobial effect of statins. *J. Antimicrobial Chemother.* **61**, 362–364 (2008).
35. Zang, Y. Y., Li, Y. M., Yin, Y., Chen, S. S. & Kai, Z. P. Discovery and quantitative structure-activity relationship study of lepidopteran HMG-CoA reductase inhibitors as selective insecticides. *Pest Manag. Sci.* **73**, 1944–1952 (2017).
36. Brain, R. A. et al. Herbicidal effects of statin pharmaceuticals in *Lemna gibba*. *Environ. Sci. Technol.* **40**, 5116–5123 (2006).
37. Shimada, T. L. et al. HIGH STEROL ESTER 1 is a key factor in plant sterol homeostasis. *Nat. Plants* **5**, 1154–1166 (2019).
38. Enjuto, M. et al. *Arabidopsis thaliana* contains two differentially expressed 3-hydroxy-3-methylglutaryl-CoA reductase genes, which encode microsomal forms of the enzyme. *Proc. Natl Acad. Sci. USA* **91**, 927–931 (1994).
39. Li, W. et al. Species-specific expansion and molecular evolution of the 3-hydroxy-3-methylglutaryl coenzyme A reductase (HMGR) gene family in plants. *PLoS ONE* **9**, e94172 (2014).
40. Vögeli, B., Shima, S., Erb, T. J. & Wagner, T. Crystal structure of archaeal HMG-CoA reductase: insights into structural changes of the C-terminal helix of the class-I enzyme. *FEBS Lett.* **593**, 543–553 (2019).
41. Peacock, R. B. et al. Structural and functional characterization of dynamic oligomerization in *Burkholderia cenocepacia* HMG-CoA reductase. *Biochemistry* **58**, 3960–3970 (2019).
42. Miller, B. R. & Kung, Y. Structural features and domain movements controlling substrate binding and cofactor specificity in class II HMG-CoA reductase. *Biochemistry* **57**, 654–662 (2018).
43. Steussy, C. N. et al. A novel role for coenzyme A during hydride transfer in 3-hydroxy-3-methylglutaryl-coenzyme A reductase. *Biochemistry* **52**, 5195–5205 (2013).

44. Sarver, R. W. et al. Thermodynamic and structure guided design of statin based inhibitors of 3-hydroxy-3-methylglutaryl coenzyme A reductase. *J. Medicinal Chem.* **51**, 3804–3813 (2008).
45. Park, W. K. et al. Hepatoselectivity of statins: design and synthesis of 4-sulfamoyl pyrroles as HMG-CoA reductase inhibitors. *Bioorg. Medicinal Chem. Lett.* **18**, 1151–1156 (2008).
46. Pfefferkorn, J. A. et al. Substituted pyrazoles as hepatoselective HMG-CoA reductase inhibitors: discovery of (3R,5R)-7-[2-(4-fluorophenyl)-4-isopropyl-5-(4-methyl-benzylcarbamoyl)-2H-pyrazol-3-yl]-3,5-dihydroxyheptanoic acid (PF-3052334) as a candidate for the treatment of hypercholesterolemia. *J. Medicinal Chem.* **51**, 31–45 (2008).
47. Pfefferkorn, J. A. et al. Design and synthesis of novel, conformationally restricted HMG-CoA reductase inhibitors. *Bioorg. Medicinal Chem. Lett.* **17**, 4531–4537 (2007).
48. Pfefferkorn, J. A. et al. Design and synthesis of hepatoselective, pyrrole-based HMG-CoA reductase inhibitors. *Bioorg. Medicinal Chem. Lett.* **17**, 4538–4544 (2007).
49. Istvan, E. S., Palnitkar, M., Buchanan, S. K. & Deisenhofer, J. Crystal structure of the catalytic portion of human HMG-CoA reductase: insights into regulation of activity and catalysis. *EMBO J.* **19**, 819–830 (2000).
50. Taberner, L., Bochar, D. A., Rodwell, V. W. & Stauffacher, C. V. Substrate-induced closure of the flap domain in the ternary complex structures provides insights into the mechanism of catalysis by 3-hydroxy-3-methylglutaryl-CoA reductase. *Proc. Natl Acad. Sci. USA* **96**, 7167–7171 (1999).
51. Oliveira, E. F., Cerqueira, N. M., Ramos, M. J. & Fernandes, P. A. QM/MM study of the mechanism of reduction of 3-hydroxy-3-methylglutaryl coenzyme A catalyzed by human HMG-CoA reductase. *Catal. Sci. Technol.* **6**, 7172–7185 (2016).
52. Tian, W., Chen, C., Lei, X., Zhao, J. & Liang, J. CASTp 3.0: computed atlas of surface topography of proteins. *Nucleic Acids Res.* **46**, W363–W367 (2018).
53. Roth, B. D. et al. Inhibitors of cholesterol biosynthesis. 1. trans-6-(2-pyrrol-1-ylethyl)-4-hydroxypyran-2-ones, a novel series of HMG-CoA reductase inhibitors. 1. Effects of structural modifications at the 2- and 5-positions of the pyrrole nucleus. *J. Medicinal Chem.* **33**, 21–31 (1990).
54. Kennedy, J. et al. Modulation of polyketide synthase activity by accessory proteins during lovastatin biosynthesis. *Science* **284**, 1368–1372 (1999).
55. Hutchinson, C. R. et al. Aspects of the biosynthesis of non-aromatic fungal polyketides by iterative polyketide synthases. *Antonie Van Leeuwenhoek* **78**, 287–295 (2000).
56. Martín, J.-F., García-Estrada, C. & Zeilinger, S. *Biosynthesis and Molecular Genetics of Fungal Secondary Metabolites* (Springer, 2014).
57. Theivagt, A. E., Amanti, E. N., Beresford, N. J., Taberner, L. & Friese, J. A. Characterization of an HMG-CoA reductase from *Listeria monocytogenes* that exhibits dual coenzyme specificity. *Biochemistry* **45**, 14397–14406 (2006).
58. Re, E. B., Jones, D. & Learned, R. M. Co-expression of native and introduced genes reveals cryptic regulation of HMG CoA reductase expression in *Arabidopsis*. *Plant J.* **7**, 771–784 (1995).
59. Marrone, P. G. Pesticidal natural products—status and future potential. *Pest Manag. Sci.* **75**, 2325–2340 (2019).
60. Haines, B. E., Wiest, O. & Stauffacher, C. V. The increasingly complex mechanism of HMG-CoA reductase. *Acc. Chem. Res.* **46**, 2416–2426 (2013).
61. Haines, B. E., Steussy, C. N., Stauffacher, C. V. & Wiest, O. Molecular modeling of the reaction pathway and hydride transfer reactions of HMG-CoA reductase. *Biochemistry* **51**, 7983–7995 (2012).
62. Abifadel, M. et al. Mutations in PCSK9 cause autosomal dominant hypercholesterolemia. *Nat. Genet.* **34**, 154–156 (2003).
63. Gaudet, D. et al. ANGPTL3 inhibition in homozygous familial hypercholesterolemia. *N. Engl. J. Med.* **377**, 296–297 (2017).
64. Hey, S. J. et al. Enhanced seed phytosterol accumulation through expression of a modified HMG-CoA reductase. *Plant Biotechnol. J.* **4**, 219–229 (2006).
65. Yan, Y. et al. Resistance-gene-directed discovery of a natural-product herbicide with a new mode of action. *Nature* **559**, 415–418 (2018).
66. Xie, L. et al. Harzianic acid from *Trichoderma afroharzianum* is a natural product inhibitor of acetohydroxyacid synthase. *J. Am. Chem. Soc.* **143**, 9575–9584 (2021).
67. Corral, M. G., Leroux, J., Stubbs, K. A. & Mylne, J. S. Herbicidal properties of antimalarial drugs. *Sci. Rep.* **7**, 1–9 (2017).
68. Haywood, J. et al. Structural basis of ribosomal peptide macrocyclization in plants. *eLife* **7**, e32955 (2018).
69. Aragao, D. et al. MX2: a high-flux undulator microfocus beamline serving both the chemical and macromolecular crystallography communities at the Australian Synchrotron. *J. Synchrotron Radiat.* **25**, 885–891 (2018).
70. Kabsch, W. XDS. *Acta Crystallogr. Section D. Biol. Crystallogr.* **66**, 125–132 (2010).
71. Winn, M. D. et al. Overview of the CCP4 suite and current developments. *Acta Crystallogr. Sect. D. Biol. Crystallogr.* **67**, 235–242 (2011).
72. McCoy, A. J. et al. Phaser crystallographic software. *J. Appl. Crystallogr.* **40**, 658–674 (2007).
73. Emsley, P., Lohkamp, B., Scott, W. G. & Cowtan, K. Features and development of Coot. *Acta Crystallogr. Sect. D. Biol. Crystallogr.* **66**, 486–501 (2010).
74. Chen, V. B. et al. MolProbity: all-atom structure validation for macromolecular crystallography. *Acta Crystallogr. Sect. D. Biol. Crystallogr.* **66**, 12–21 (2010).
75. Curtis, M. D. & Grossniklaus, U. A gateway cloning vector set for high-throughput functional analysis of genes *in planta*. *Plant Physiol.* **133**, 462–469 (2003).
76. Clough, S. J. & Bent, A. F. Floral dip: a simplified method for *Agrobacterium*-mediated transformation of *Arabidopsis thaliana*. *Plant J.* **16**, 736–743 (1998).
77. Bechtold, N., Ellis, J. & Pelletier, G. In planta *Agrobacterium*-mediated gene transfer by infiltration of adult *Arabidopsis thaliana* plants. *Comptes rendus de l'Académie des. Sci. Série III, Sci. de. la vie* **316**, 1194–1199 (1993).

Acknowledgements

The authors thank Grishma Vadlamani and Yit-Heng Chooi for their helpful comments. This research was undertaken in part using the MX2 beamline at the Australian Synchrotron, part of The Australian Nuclear Science and Technology Organisation, and made use of the Australian Cancer Research Foundation detector. J.H. was supported by an Australian Research Council Discovery Early Career Researcher Award (DE180101445) and funded in part by Nexgen Plants. This work was supported by an Australian Research Council Discovery Project DP190101048 to J.S.M., K.A.S. and J.H. and an ARC Linkage Infrastructure Equipment and Facilities Grant (LE190100123) to K.A.S.

Author contributions

J.H. and J.S.M. designed and coordinated the research. J.H., J.Z. and K.J.B. performed plant assays. K.J.B. and K.A.S. designed and synthesised atorvastatin analogues. M.T.W. made binary constructs used by J.H. and J.S.M. for plant transgenesis. J.H. analysed transgenic lines, made recombinant proteins, performed assays, and acquired crystals. J.H. and C.S.B. solved crystal structures. J.H. and J.S.M. wrote the manuscript with input from all authors.

Competing interests

The authors declare no competing interests.

Additional information

Supplementary information The online version contains supplementary material available at <https://doi.org/10.1038/s41467-022-33185-0>.

Correspondence and requests for materials should be addressed to Joel Haywood or Joshua S. Mylne.

Peer review information *Nature Communications* thanks Stephen Duke and the other, anonymous, reviewer(s) for their contribution to the peer review of this work.

Reprints and permission information is available at <http://www.nature.com/reprints>

Publisher's note Springer Nature remains neutral with regard to jurisdictional claims in published maps and institutional affiliations.

Open Access This article is licensed under a Creative Commons Attribution 4.0 International License, which permits use, sharing, adaptation, distribution and reproduction in any medium or format, as long as you give appropriate credit to the original author(s) and the source, provide a link to the Creative Commons license, and indicate if changes were made. The images or other third party material in this article are included in the article's Creative Commons license, unless indicated otherwise in a credit line to the material. If material is not included in the article's Creative Commons license and your intended use is not permitted by statutory regulation or exceeds the permitted use, you will need to obtain permission directly from the copyright holder. To view a copy of this license, visit <http://creativecommons.org/licenses/by/4.0/>.

© The Author(s) 2022